Parametric instability, inverse cascade and the $1/f$ range of solar-wind turbulence

Benjamin D. G. Chandran†

Department of Physics, University of New Hampshire, Durham, New Hampshire 03824, USA

In this paper, weak-turbulence theory is used to investigate the nonlinear evolution of the parametric instability in three-dimensional low-β plasmas at wavelengths much greater than the ion inertial length under the assumption that slow magnetosonic waves are strongly damped. It is shown analytically that the parametric instability leads to an inverse cascade of Alfvén wave quanta, and several exact solutions to the wave kinetic equations are presented. The main results of the paper concern the parametric decay of Alfvén waves that initially satisfy $e^+ \gg e^-$, where e^+ and e^- are the frequency (f) spectra of Alfvén waves propagating in opposite directions along the magnetic field lines. If e^+ initially has a peak frequency f_0 (at which fe^+ is maximized) and an 'infrared' scaling f^p at smaller f with $-1 < p < 1$, then e^+ acquires an f^{-1} scaling throughout a range of frequencies that spreads out in both directions from f_0. At the same time, e^- acquires an f^{-2} scaling within this same frequency range. If the plasma parameters and infrared e^+ spectrum are chosen to match conditions in the fast solar wind at a heliocentric distance of 0.3 astronomical units (AU), then the nonlinear evolution of the parametric instability leads to an e^+ spectrum that matches fast-wind measurements from the *Helios* spacecraft at 0.3 AU, including the observed f^{-1} scaling at $f \gtrsim 3 \times 10^{-4}$ Hz. The results of this paper suggest that the f^{-1} spectrum seen by *Helios* in the fast solar wind at $f \gtrsim 3 \times 10^{-4}$ Hz is produced *in situ* by parametric decay and that the f^{-1} range of e^+ extends over an increasingly narrow range of frequencies as r decreases below 0.3 AU. This prediction will be tested by measurements from the Parker Solar Probe.

Key words: astrophysical plasmas, plasma nonlinear phenomena, plasma waves

1. Introduction

The origin of the solar wind is a long-standing problem (Parker 1958) that continues to receive considerable attention. A leading model for the origin of the fast solar wind appeals to Alfvén waves (AWs) that are launched by photospheric motions. As these AWs propagate away from the Sun, they undergo partial reflection due to the radial variation of the Alfvén speed (Heinemann & Olbert 1980). Nonlinear interactions between counter-propagating AWs then cause AW energy to cascade to small

† Email address for correspondence: benjamin.chandran@unh.edu

scales and dissipate, heating the plasma (Velli, Grappin & Mangeney 1989; Zhou & Matthaeus 1989; Cranmer & van Ballegooijen 2005; Verdini *et al.* 2012; Perez & Chandran 2013; van Ballegooijen & Asgari-Targhi 2017). This heating increases the plasma pressure, which, in conjunction with the wave pressure, accelerates the plasma to high speeds (Suzuki & Inutsuka 2005; Cranmer, van Ballegooijen & Edgar 2007; Verdini *et al.* 2010; Chandran *et al.* 2011; van der Holst *et al.* 2014).

Although non-compressive AWs are the primary mechanism for energizing the solar wind in this model, a number of considerations indicate that compressive fluctuations have a significant impact on the dynamics of turbulence in the corona and solar wind. Observations of the tail of Comet-Lovejoy reveal that the background plasma density ρ_0 at $r = 1.2 R_\odot$ (where $R_\odot$ is the radius of the Sun) varies by a factor of ~ 6 over distances of a few thousand km measured perpendicular to the background magnetic field $\boldsymbol{B}_0$ (Raymond *et al.* 2014). These density variations (denoted $\delta\rho$) lead to phase mixing of AWs, which transports AW energy to smaller scales measured perpendicular to $\boldsymbol{B}_0$ (Heyvaerts & Priest 1983). Farther from the Sun, where $\delta\rho/\rho_0$ is significantly smaller than $|\delta\boldsymbol{B}|/B_0$ (Tu & Marsch 1995; Hollweg, Cranmer & Chandran 2010), AWs still couple to slow magnetosonic waves ('slow waves') through the parametric instability, in which outward-propagating AWs decay into outward-propagating slow waves and inward-propagating AWs[1] (Galeev & Oraevskii 1963; Sagdeev & Galeev 1969; Goldstein 1978; Spangler 1986, 1989, 1990; Hollweg 1994; Dorfman & Carter 2016). This instability and its nonlinear evolution are the focus of the present work.

A number of studies have investigated the parametric instability in the solar wind within the framework of magnetohydrodynamics (MHD) (e.g. Malara, Primavera & Veltri 2000; Del Zanna, Velli & Londrillo 2001; Shi *et al.* 2017), while others have gone beyond MHD to account for temperature anisotropy (Tenerani, Velli & Hellinger 2017) or kinetic effects such as the Landau damping of slow waves (e.g. Inhester 1990; Vasquez 1995; Araneda, Marsch & Viñas 2008; Maneva, Viñas & Ofman 2013). Cohen & Dewar (1974), for example, derived the growth rate of the parametric instability in the presence of strong slow-wave damping and randomly phased, parallel-propagating AWs. Terasawa *et al.* (1986) carried out one-dimensional (1-D) hybrid simulations and found that Landau damping reduces the growth rate of the parametric instability and that the parametric instability leads to an inverse cascade of AWs to smaller frequencies.

In this paper, weak-turbulence theory is used to investigate the nonlinear evolution of the parametric instability assuming a randomly phased collection of AWs at wavelengths much greater than the proton inertial length d_i in a low-β plasma, where β is the ratio of plasma pressure to magnetic pressure. The fluctuating fields are taken to depend on all three spatial coordinates, but the wave kinetic equations are integrated over the perpendicular (to $\boldsymbol{B}_0$) wave-vector components, yielding equations for the 1-D power spectra that depend only on the parallel wavenumber and time. The starting point of the analysis is the theory of weak compressible MHD turbulence. Collisionless damping of slow waves is incorporated in a very approximate manner analogous to the approach of Cohen & Dewar (1974), by dropping terms containing the slow-wave energy density in the wave kinetic equations that describe the evolution of the AW power spectra.

The remainder of the paper is organized as follows. Section 2 reviews results from the theory of weak compressible MHD turbulence, and § 3 uses the weak-turbulence

---

[1]The terms outward-propagating and inward-propagating refer to the propagation direction in the plasma rest frame. Beyond the Alfvén critical point, all AWs propagate outward in the rest frame of the Sun.

wave kinetic equations to recover the results of Cohen & Dewar (1974) in the linear regime. Section 4 shows how the wave kinetic equations imply that AW quanta undergo an inverse cascade towards smaller parallel wavenumbers, and §5 presents several exact solutions to the wave kinetic equations. The main results of the paper appear in §6, which uses a numerical solution and an approximate analytic solution to the wave kinetic equations to investigate the parametric decay of an initial population of randomly phased AWs propagating in the same direction with negligible initial power in counter-propagating AWs. The numerical results are compared with observations from the *Helios* spacecraft at a heliocentric distance of 0.3 astronomical units (AU). Section 7 critically revisits the main assumptions of the analysis and the relevance of the analysis to the solar wind. Section 8 summarizes the key findings of the paper, including predictions that will be tested by NASA's Parker Solar Probe.

2. The wave kinetic equations for Alfvén waves undergoing parametric decay

In weak-turbulence theory, the quantity $\omega_{nl}/\omega_{linear}$ is treated as a small parameter, where ω_{nl} is the inverse of the time scale on which nonlinear interactions modify the fluctuations, and ω_{linear} is the linear wave frequency. Because

$$\omega_{nl} \ll \omega_{linear}, \tag{2.1}$$

the fluctuations can be viewed as waves to a good approximation. The governing equations lead to a hierarchy of equations for the moments of various fluctuating quantities, in which the time derivatives of the second moments (or second-order correlation functions) depend upon the third moments, and the time derivatives of the third moments depend upon the fourth moments, and so on. This system of equations is closed via the random-phase approximation, which allows the fourth-order correlation functions to be expressed as products of second-order correlation functions (see, e.g. Galtier *et al.* 2000).

The strongest nonlinear interactions in weak MHD turbulence are resonant three-wave interactions. These interactions occur when the frequency and wavenumber of the beat wave produced by two waves is identical to the frequency and wavenumber of some third wave, which enables the beat wave to drive the third wave coherently in time. If the three waves have wavenumbers $\boldsymbol{p}$, $\boldsymbol{q}$, and $\boldsymbol{k}$ and frequencies ω_p, ω_q, and ω_k, respectively, then a three-wave resonance requires that

$$\boldsymbol{k} = \boldsymbol{p} + \boldsymbol{q}, \tag{2.2}$$

and

$$\omega_k = \omega_p + \omega_q. \tag{2.3}$$

An alternative interpretation of (2.2) and (2.3) arises from viewing the wave fields as a collection of wave quanta at different wavenumbers and frequencies, restricting the frequencies to positive values, and assigning a wave quantum at wavenumber $\boldsymbol{k}$ and frequency ω_k the momentum $\hbar\boldsymbol{k}$ and energy $\hbar\omega_k$. Equations (2.2) and (2.3) then correspond to the momentum-conservation and energy-conservation relations that arise when either one wave quantum decays into two new wave quanta or two wave quanta merge to produce a new wave quantum.

In the parametric instability in a low-β plasma, a parent AW (or AW quantum) at wavenumber $\boldsymbol{k}$ decays into a slow wave at wavenumber $\boldsymbol{p}$ propagating in the same direction and an AW at wavenumber $\boldsymbol{q}$ propagating in the opposite direction.

Regardless of the direction of the wave vector, the group velocity of an AW is either parallel or anti-parallel to the background magnetic field

$$\boldsymbol{B}_0 = B_0 \hat{z}, \tag{2.4}$$

and the same is true for slow waves when

$$\beta \ll 1, \tag{2.5}$$

which is henceforth assumed. At low β slow waves travel along field lines at the sound speed c_s, which is approximately $\beta^{1/2}$ times the Alfvén speed v_A. Thus, regardless of the perpendicular components of $\boldsymbol{k}$, $\boldsymbol{p}$, and $\boldsymbol{q}$, the frequency-matching condition (2.3) for the parametric instability is

$$k_z v_A = p_z c_s - q_z v_A. \tag{2.6}$$

Combining the z component of (2.2) with (2.6) and taking $c_s \ll v_A$ yields

$$p_z \simeq 2k_z, \tag{2.7}$$

and

$$q_z \simeq -k_z \left(1 - \frac{2c_s}{v_A} \right). \tag{2.8}$$

Equation (2.8) implies that the frequency $|q_z v_A|$ of the daughter AW is slightly smaller than the frequency $|k_z v_A|$ of the parent AW (Sagdeev & Galeev 1969). Thus, the energy of the daughter AW is slightly smaller than the energy of the parent AW. This reduction in AW energy is offset by an increase in slow-wave energy.

Chandran (2008) derived the wave kinetic equations for weakly turbulent AWs, slow waves, and fast magnetosonic waves ('fast waves') in the low-β limit. The resulting equations were expanded in powers of β, and only the first two orders in the expansion (proportional to β^{-1} and β^0, respectively) were retained. Slow waves are strongly damped in collisionless low-β plasmas (Barnes 1966). Chandran (2008) neglected collisionless damping during the derivation of the wave kinetic equations, but incorporated it afterward in an *ad hoc* manner by assuming that the slow-wave power spectrum $S_k^\pm$ was small and discarding terms $\propto S_k^\pm$ unless they were also proportional to β^{-1}.[2] (The $\pm$ sign in $S_k^\pm$ indicates slow waves propagating parallel ($+$) or anti-parallel ($-$) to $\boldsymbol{B}_0$.)

In the present paper, the wave kinetic equations derived by Chandran (2008) are used to investigate the nonlinear evolution of the parametric instability. It is assumed that slow-wave damping is sufficiently strong that all terms $\propto S_k^\pm$, even those $\propto \beta^{-1}$, can be safely discarded. All other types of nonlinear interactions are neglected, including resonant interactions between three AWs, phase mixing and resonant interactions involving fast waves. Given these approximations, equation (8) of Chandran (2008) becomes

$$\frac{\partial A_k^\pm}{\partial t} = \frac{\pi}{v_A} \int d^3p \, d^3q \, \delta(\boldsymbol{k} - \boldsymbol{p} - \boldsymbol{q}) \delta(q_z + k_z) k_z^2 A_k^\pm \frac{\partial}{\partial q_z}(q_z A_q^\mp), \tag{2.9}$$

[2]The one exception to this rule was that Chandran (2008) retained the term representing turbulent mixing of slow waves by AWs, since this term can dominate the evolution of slow waves at small k_z (Lithwick & Goldreich 2001; Schekochihin *et al.* 2016).
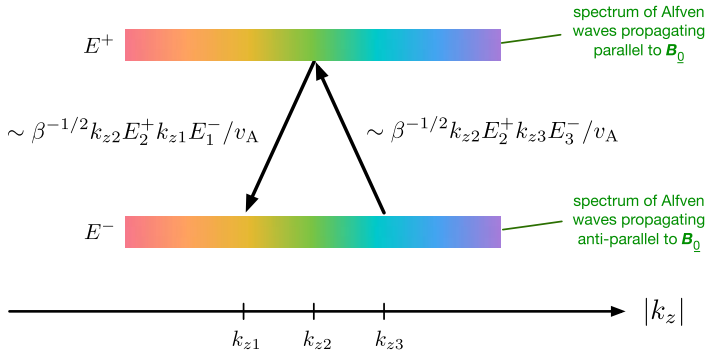
FIGURE 1. Physical interpretation of the wave kinetic equation for parametric decay when slow waves are strongly damped (2.11). The mathematical expressions next to the arrows represent the contributions to $\partial E^+(k_{z2})/\partial t$ from the parametric decay of AWs at k_{z3}, which acts to increase $E^+(k_{z2})$, and the parametric decay of AWs at k_{z2}, which acts to decrease $E^+(k_{z2})$. In these expressions, $E_2^+ = E^+(k_{z2})$, $E_1^- = E^-(k_{z1})$, and $E_3^- = E^-(k_{z3})$.

where A_k^+ (A_k^-) is the 3-D wavenumber spectrum of AWs propagating parallel (anti-parallel) to $\boldsymbol{B}_0$, $\delta(x)$ is the Dirac delta function, and the integral over each Cartesian component of $\boldsymbol{p}$ and $\boldsymbol{q}$ extends from $-\infty$ to $+\infty$. The 3-D AW power spectra depend upon all three wave-vector components and time. The $\delta(\boldsymbol{k} - \boldsymbol{p} - \boldsymbol{q})$ term enforces the wavenumber-resonance condition (2.2), and the $\delta(q_z + k_z)$ term enforces the frequency-resonance condition (2.8) to leading order in β. The integral over the components of $\boldsymbol{p}$ in (2.9) can be carried out immediately, thereby annihilating the first delta function. Equation (2.9) can be further simplified by introducing the 1-D wavenumber spectra

$$E^\pm(k_z, t) = \int_{-\infty}^\infty \mathrm{d}k_x \int_{-\infty}^\infty \mathrm{d}k_y A_k^\pm, \tag{2.10}$$

and integrating (2.9) over k_x and k_y, which yields

$$\frac{\partial E^\pm}{\partial t} = \frac{\pi}{v_A} k_z^2 E^\pm \frac{\partial}{\partial k_z}(k_z E^\mp). \tag{2.11}$$

Equation (2.11) describes how the 1-D (parallel) power spectra $E^\pm$ evolve and forms the basis for much of the discussion to follow. Given the aforementioned assumptions, the evolution of the 1-D power spectra $E^\pm$ is not influenced by the way that $A^\pm$ depends on k_x and k_y. For future reference, the normalization of the power spectra is such that

$$\int_{-\infty}^\infty \mathrm{d}k_z E^\pm = \frac{1}{2}\left\langle \left| \delta \boldsymbol{v}_{AW} \mp \frac{\delta \boldsymbol{B}_{AW}}{\sqrt{4\pi\rho}} \right|^2 \right\rangle, \tag{2.12}$$

where $\delta \boldsymbol{v}_{AW}$ and $\delta \boldsymbol{B}_{AW}$ are the velocity and magnetic-field fluctuations associated with AWs, and $\langle \cdots \rangle$ indicates an average over space and time (Chandran 2008).

2.1. *Physical interpretation of the wave kinetic equation*

Figure 1 offers a way of understanding (2.11). The horizontal colour bars in this figure represent the spectra of outward-propagating and inward-propagating AWs, with red representing longer-wavelength waves and violet representing shorter-wavelength waves. AWs propagating in the $-\boldsymbol{B}_0$ direction at $|k_z| = k_{z3}$ decay into slow waves

propagating anti-parallel to B_0 at $|k_z| \simeq 2k_{z3}$ and AWs propagating parallel to B_0 at $|k_z| = k_{z2}$. AWs propagating parallel to B_0 at $|k_z| = k_{z2}$ decay into slow waves propagating parallel to B_0 at $|k_z| \simeq 2k_{z2}$ and AWs propagating anti-parallel to B_0 at $|k_z| = k_{z1}$. Equation (2.11) is approximately equivalent to the statement that the rate at which $E_2^+ = E^+(k_{z2})$ increases via the decay of AWs at $|k_z| = k_{z3}$ is

$$R_{3 \rightarrow 2} \sim \frac{k_{z2} E_2^+ k_{z3} E_3^-}{\beta^{1/2} v_A}, \tag{2.13}$$

where $E_3^- = E^-(k_{z3})$, while the rate at which E_2^+ decreases via the decay of AWs at $|k_z| = k_{z2}$ is

$$R_{2 \rightarrow 1} \sim \frac{k_{z2} E_2^+ k_{z1} E_1^-}{\beta^{1/2} v_A}, \tag{2.14}$$

where $E_1^- = E^-(k_{z1})$. The time derivative of E_2^+ is $R_{3 \rightarrow 2} - R_{2 \rightarrow 1}$, or

$$\frac{\partial E_2^+}{\partial t} \sim \frac{k_{z2} E_2^+ (k_{z3} E_3^- - k_{z1} E_1^-)}{\beta^{1/2} v_A}. \tag{2.15}$$

Equation (2.8) implies that $k_{z3} - k_{z1} \sim k_{z2} c_s / v_A \sim \beta^{1/2} k_{z2}$. A Taylor expansion of $k_{z3} E_3^-$ and $k_{z1} E_1^-$ about k_{z2} in (2.15) thus allows this equation to be rewritten as

$$\frac{\partial E_2^+}{\partial t} \sim \frac{k_{z2}^2 E_2^+}{v_A} \frac{\partial}{\partial k_z} (k_z E^-) \bigg|_{k_z = k_{z2}}, \tag{2.16}$$

which is the same as (2.11) to within a factor of order unity.

To be clear, no independent derivation is being presented for (2.13) and (2.14). The foregoing discussion merely points out that (2.13) and (2.14) are equivalent (up to a factor of order unity) to (2.11), which is derived on the basis of weak-turbulence theory. It is worth pointing out, however, that several features of (2.13) and (2.14) make sense on a qualitative level. If either $E^+ = 0$ or $E^- = 0$, then $R_{3 \rightarrow 2} = R_{2 \rightarrow 1} = 0$, because the parametric instability is a stimulated decay, which ceases if initially all the AWs travel in the same direction. For fixed E^+ and E^-, $R_{3 \rightarrow 2}$ and $R_{2 \rightarrow 1}$ vanish as $v_A \rightarrow \infty$, since the fractional nonlinearities vanish in this limit. Also, $R_{3 \rightarrow 2}$ and $R_{2 \rightarrow 1}$ are proportional to $\beta^{-1/2}$ (when $S_k^\pm$ is negligibly small, as assumed) because the parametric-decay contribution to $\partial A_k^\pm / \partial t$ is an integral (over p and q) of third-order correlation functions such as $\langle \delta v_k \cdot \delta B_q \delta n_p \rangle$, where δv_k and δB_q are the velocity and magnetic-field fluctuations associated with AWs at wave vectors k and q, and δn_p is the density fluctuation associated with the slow waves at wave vector p that are driven by the beating of the AWs at wave vectors k and q. For fixed AW amplitudes and fixed B_0 and v_A, this driven density fluctuation is proportional to $\beta^{-1/2}$, because as β decreases the thermal pressure is less able to resist the compression along B_0 resulting from the Lorentz force that arises from the beating of the AWs.

3. Linear growth of the parametric instability

In the linear regime of the parametric instability, the spectrum of AWs propagating in one direction, say E^+, is taken to be fixed, and $E^- \ll E^+$. Equation (2.11) then implies that E^- increases exponentially in time with growth rate

$$\gamma^- = \frac{\pi k_z^2}{v_A} \frac{\partial}{\partial k_z} (k_z E^+). \tag{3.1}$$

Equation (3.1) is equivalent to equation (18) of Cohen & Dewar (1974) given the different normalizations of the AW power spectra in the two equations. For example, equation (2.12) implies that $\int_0^\infty E^+ \, dk_z = (1/2) \int_{-\infty}^\infty E^+ \, dk_z = \langle |\delta \boldsymbol{B}|^2 \rangle / 4\pi\rho$ when $E^- \ll E^+$, which can be compared with the un-numbered but displayed equation under equation (9) of Cohen & Dewar (1974). As in the present paper, Cohen & Dewar (1974) assumed that slow waves are strongly damped and that the AWs satisfy the random-phase approximation. The present paper builds upon the results of Cohen & Dewar (1974) by investigating the coupled nonlinear evolution of E^+ and E^-. Also, whereas Cohen & Dewar (1974) took the wave vectors to be parallel or anti-parallel to $\boldsymbol{B}_0$, the derivation of (2.11) in the present paper allows for obliquely propagating waves.

4. Conservation of wave quanta and inverse cascade

To simplify the presentation, it is assumed that

$$k_z > 0. \tag{4.1}$$

No generality is lost, because $E^\pm$ is an even function of k_z, and thus it is sufficient to solve for the spectra at positive k_z values. Equation (2.11) can be rewritten as the two equations

$$\frac{\partial N}{\partial t} + \frac{\partial \Gamma}{\partial k_z} = 0 \tag{4.2}$$

and

$$\frac{\partial \Gamma}{\partial t} = \pi \hbar k_z^2 \Gamma \frac{\partial}{\partial k_z} (k_z^2 N), \tag{4.3}$$

where

$$N = \frac{E^+ + E^-}{\hbar k_z v_A} \tag{4.4}$$

is the number of wave quanta per unit k_z per unit mass and

$$\Gamma = -\frac{\pi k_z^2 E^+ E^-}{\hbar v_A^2} \tag{4.5}$$

is the flux of wave quanta in k_z-space. Equation (4.2) implies that the number of wave quanta per unit mass,

$$N_{\text{tot}} = \int_{-\infty}^\infty N \, dk_z, \tag{4.6}$$

is conserved. The fact that Γ is negative indicates that there is an inverse cascade of wave quanta from large k_z to small k_z (cf. Terasawa *et al.* 1986). The wavenumber drift velocity of the wave quanta,

$$\left\langle \frac{dk_z}{dt} \right\rangle \equiv \frac{\Gamma}{N} = -\frac{\pi k_z^3}{v_A} \left(\frac{1}{E^+} + \frac{1}{E^-} \right)^{-1}, \tag{4.7}$$

is determined primarily by the smaller of E^+ and E^-.

5. Exact solutions to the wave kinetic equations

In this section, several exact solutions to (2.11) are presented under the assumption that $k_z > 0$. The spectra at negative k_z follow from the relation $E^\pm(-k_z, t) = E^\pm(k_z, t)$.

5.1. *Decaying, balanced turbulence*

One family of exact solutions to (2.11) follows from setting

$$E^{\pm}(k_z, t) = f^{\pm}(k_z, t) H(k_z - b(t)) \tag{5.1}$$

in (2.11), where

$$H(x) = \begin{cases} 0 & \text{if } x < 0, \\ 1 & \text{if } x \geqslant 0, \end{cases} \tag{5.2}$$

is the Heaviside function. When (5.1) is substituted into (2.11), each side of (2.11) becomes the sum of terms proportional to $\delta(k_z - b)$ and terms that contain no delta function. By separately equating the two groups of terms, one can show that (5.1) is a solution to (2.11) if

$$\frac{\partial}{\partial t} f^{\pm}(k_z, t) = \frac{\pi}{v_A} k_z^2 f^{\pm}(k_z, t) \frac{\partial}{\partial k_z} [k_z f^{\mp}(k_z, t)], \tag{5.3}$$

and

$$\frac{1}{b^3} \frac{db}{dt} = -\frac{\pi f^+(b, t)}{2 v_A} = -\frac{\pi f^-(b, t)}{2 v_A}. \tag{5.4}$$

Equation (5.4) makes use of the relation $[H(x)]^2 = H(x)$ and its derivative, $2H(x)\delta(x) = \delta(x)$. In appendix A it is shown that (5.4) can be recovered by adding a small amount of nonlinear diffusion to (2.11) and replacing the discontinuous jump in the spectrum at $k_z = b(t)$ with a boundary layer. Equation (5.4) implies that, for solutions of the form given in (5.1), the mean-square amplitudes of forward- and backward-propagating AWs must be equal just above the break wavenumber b. An exact solution to (5.3) and (5.4) corresponding to decaying turbulence is

$$f^+(k_z, t) = f^-(k_z, t) = \frac{a(t)}{k_z^2}, \tag{5.5}$$

$$a(t) = a_0 \left(1 + \frac{\pi a_0 t}{v_A} \right)^{-1}, \tag{5.6}$$

and

$$b(t) = b_0 \left(1 + \frac{\pi a_0 t}{v_A} \right)^{-1/2}, \tag{5.7}$$

where a_0 and b_0 are the values of a and b at $t = 0$.

This solution can be further truncated at large k_z by setting

$$E^+(k_z, t) = E^-(k_z, t) = \frac{a(t) H(k_z - b(t)) H(q(t) - k_z)}{k_z^2} \tag{5.8}$$

with

$$q(t) = q_0 \left(1 + \frac{\pi a_0 t}{v_A} \right)^{-1/2}, \tag{5.9}$$

where q_0 is the value of q at $t = 0$, which is taken to exceed b_0. Equations (5.5) through (5.9) can be recovered numerically by solving (2.11) for freely decaying AWs. Whether the spectra satisfy (5.1) and (5.5) through (5.7) or, alternatively, equations (5.6) through (5.9), the number of wave quanta N_{tot} defined in (4.6) is finite and independent of time.

5.2. *Forced, balanced turbulence*

An exact solution to (5.3) and (5.4) corresponding to forced turbulence is

$$f^+(k_z, t) = f^-(k_z, t) = \frac{c}{k_z}, \tag{5.10}$$

and

$$b(t) = \left(\frac{\pi c t}{2 v_{\text{A}}} + \frac{1}{b_0}\right)^{-1}, \tag{5.11}$$

where c is a constant and b_0 is the value of b at $t = 0$. In this solution, the number of wave quanta N_{tot} is not constant, because there is a non-zero influx of wave quanta from infinity. A version of this solution can be realized in a numerical solution of (2.11) by holding $E^\pm$ fixed at some wavenumber k_{f}, which mimics the effects of energy input from external forcing. In this case, the numerical solution at $k_z < k_{\text{f}}$ is described by (5.1), (5.10) and (5.11), with $b(t) < k_{\text{f}}$.

The solution in (5.10) and (5.11) can be truncated at large k_z in a manner analogous to (5.8), but with $q = [(\pi c t/2 v_{\text{A}}) + (1/q_0)]^{-1}$, where q_0 is the value of q at $t = 0$. In this solution, N_{tot} is independent of time. Numerical solutions of (2.11) show, however, that this solution is unstable. If the spectra initially satisfy $E^\pm = (c/k_z)H(k_z - b)H(q - k_z)$, then they evolve towards the solution described by (5.5) through (5.9).

5.3. *Exact solutions extending over all k_z*

In addition to the truncated solutions described in §§ 5.1 and 5.2, equation (2.11) possesses several exact solutions that extend over all k_z. These solutions are unphysical, because they correspond to infinite AW energy and neglect dissipation (which becomes important at sufficiently large k_z) and finite system size (which becomes important at sufficiently small k_z). However, they illustrate several features of the nonlinear evolution of the parametric instability, which are summarized at the end of this section.

The simplest solution to (2.11) spanning all k_z is

$$E^\pm(k_z, t) = \frac{c^\pm}{k_z}, \tag{5.12}$$

where $c^\pm$ is a constant. It follows from (4.5) that (5.12) corresponds to a constant flux of AW quanta to smaller k_z. In contrast to the truncated $E^\pm \propto k_z^{-1}$ forced-turbulence solution in § 5.2, E^+ and E^- need not be equal in (5.12).

A second, non-truncated, exact solution to (2.11) is given by

$$E^\pm(k_z, t) = \frac{a^\pm(t)}{k_z^2}, \tag{5.13}$$

and

$$a^\pm(t) = \frac{a_0^\pm(a_0^\pm - a_0^\mp)}{a_0^\pm - a_0^\mp e^{-\pi(a_0^\pm - a_0^\mp)t/v_{\text{A}}}}, \tag{5.14}$$

where a_0^+ and a_0^- are the initial values of a^+ and a^-. In this solution,

$$a^+(t) - a^-(t) = a_0^+ - a_0^-. \tag{5.15}$$

If $a_0^+ > a_0^-$, then E^- decays faster than E^+, and, after a long time has passed, E^- decays to zero while a^+ decays to the value $a_0^+ - a_0^-$. Conversely, if $a_0^- > a_0^+$, then E^+ decays faster than E^-, and the turbulence decays to a state in which $E^+ = 0$. In the limit that $a_0^+ \to a_0^-$,

$$a^\pm(t) \to a_0 \left(1 + \frac{\pi a_0 t}{v_A} \right)^{-1}, \tag{5.16}$$

where $a_0 = a_0^+ = a_0^-$. Equations (5.13) and (5.16) are a non-truncated version of the decaying-turbulence solution presented in § 5.1.

Equations (5.12) and (5.13) can be combined into a more general class of solution,

$$E^\pm(k_z, t) = a^\pm(t) \left(\frac{1}{k_z^2} + \frac{d^\pm}{k_z} \right), \tag{5.17}$$

where d^+ and d^- are constants and $a^\pm(t)$ is given by (5.14). Another type of solution combining k_z^{-1} and k_z^{-2} scalings is

$$E^+(k_z, t) = \frac{c_0 e^{-\pi c_2 t/v_A}}{k_z}, \tag{5.18}$$

$$E^-(k_z, t) = \frac{c_1}{k_z} + \frac{c_2}{k_z^2}, \tag{5.19}$$

where c_0, c_1, and c_2 are constants.

The exact solutions presented in this section illustrate three properties of the nonlinear evolution of the parametric instability at low β when slow waves are strongly damped. First, when $E^\pm \propto k_z^{-1}$, $\partial E^\mp/\partial t$ vanishes. Second, if $E^\pm \propto k_z^{-2}$, then $(\partial/\partial t) \ln E^\mp$ is negative and independent of k_z, and $E^\mp(k_z, t)$ can be written as the product of a function of k_z and a (decreasing) function of time. (More general principles describing the evolution of $E^\pm$ are summarized in figure 3 and (6.11).) Third, the parametric instability does not necessarily saturate with $E^+ = E^-$. For example, in (5.13) and (5.14), when $a_0^+ \neq a_0^-$, the AWs decay to a maximally aligned state reminiscent of the final state of decaying cross-helical incompressible MHD turbulence (Dobrowolny, Mangeney & Veltri 1980).

6. Nonlinear evolution of the parametric instability when most of the AWS initially propagate in the same direction

This section describes a numerical solution to (2.11) in which, initially,

$$E^+ \gg E^-. \tag{6.1}$$

As in § 5, k_z is taken to be positive, and the spectra at negative k_z can be inferred from the fact that $E^\pm(-k_z) = E^\pm(k_z)$. The spectra are advanced forward in time using a second-order Runge–Kutta algorithm on a logarithmic wavenumber grid consisting of 2000 grid points. To prevent the growth of numerical instabilities, a nonlinear diffusion term

$$D^\pm = \nu E^\mp k_z^2 \frac{\partial^2}{\partial k_z^2} E^\pm \tag{6.2}$$

is added to the right-hand side of (2.11), where ν is a constant. The value of ν is chosen as small as possible subject to the constraint that the diffusion term suppress instabilities at the grid scale.

To represent the solution in a way that can be readily compared with spacecraft measurements of solar-wind turbulence, the wavenumber spectra are converted into frequency spectra,

$$e^{\pm}(f, t) = \frac{2\pi E^{\pm}(k_z, t)}{U}, \tag{6.3}$$

where U is the solar-wind velocity, and

$$f = \frac{k_z U}{2\pi} \tag{6.4}$$

is the frequency in the spacecraft frame that, according to Taylor's (1938) hypothesis, corresponds to wavenumber k_z when the background magnetic field is aligned with the nearly radial solar-wind velocity. The Alfvén speed is taken to be the approximate average of the observed values of v_A in three fast-solar-wind streams at $r = 0.3$ AU (see table 1 of Marsch *et al.* (1982) and table 1a of Marsch & Tu (1990)),

$$v_A = 150 \text{ km s}^{-1}. \tag{6.5}$$

In order to compare directly with figure 2–2(*c*) of Tu & Marsch (1995), the solar-wind velocity is taken to be

$$U = 733 \text{ km s}^{-1}. \tag{6.6}$$

The power spectra are initialized to the values

$$e^+(f, t = 0) = \frac{\sigma^+ (f/f_0)^{-0.5}}{1 + (f/f_0)^{1.5}}, \tag{6.7}$$

and

$$e^-(f, t = 0) = \sigma^-, \tag{6.8}$$

where σ^+, σ^- and f_0 are constants. The values of f_0 and the corresponding wavenumber k_{z0} are chosen so that

$$f_0 = \frac{k_{z0} U}{2\pi} = 10^{-2} \text{ Hz}, \tag{6.9}$$

consistent with the arguments of van Ballegooijen & Asgari-Targhi (2016) about the dominant frequency of AW launching by the Sun. The minimum and maximum wavenumbers of the numerical domain are chosen so that $k_{z\max} = 10^3 k_{z0} = 10^7 k_{z\min}$. The motivation for the scaling $e^+(f, t = 0) \propto f^{-0.5}$ at small f is the similar scaling observed by Tu & Marsch (1995) in the aforementioned fast-solar-wind stream at 10^{-5} Hz $< f < 10^{-4}$ Hz. The numerical results shown below suggest that the parametric instability has little effect on e^+ at these frequencies at $r = 0.3$ AU. The observed $f^{-0.5}$ scaling in this frequency range is thus presumably inherited directly from the spectrum of AWs launched by the Sun. Like the scaling $e^+ \propto f^{-0.5}$, the value of σ^+ is chosen to match the observed spectrum of outward-propagating AWs at 0.3 AU at small f. The reason for the f^{-2} scaling in e^+ at large f is that a (parallel) k_z^{-2} spectrum is observed in the solar wind (Horbury, Forman & Oughton 2008; Podesta 2009; Forman, Wicks & Horbury 2011) and predicted by the theory of critically balanced MHD turbulence (see, e.g. Goldreich & Sridhar 1995; Mallet, Schekochihin & Chandran 2015). The value of σ^- is set equal to a minuscule value
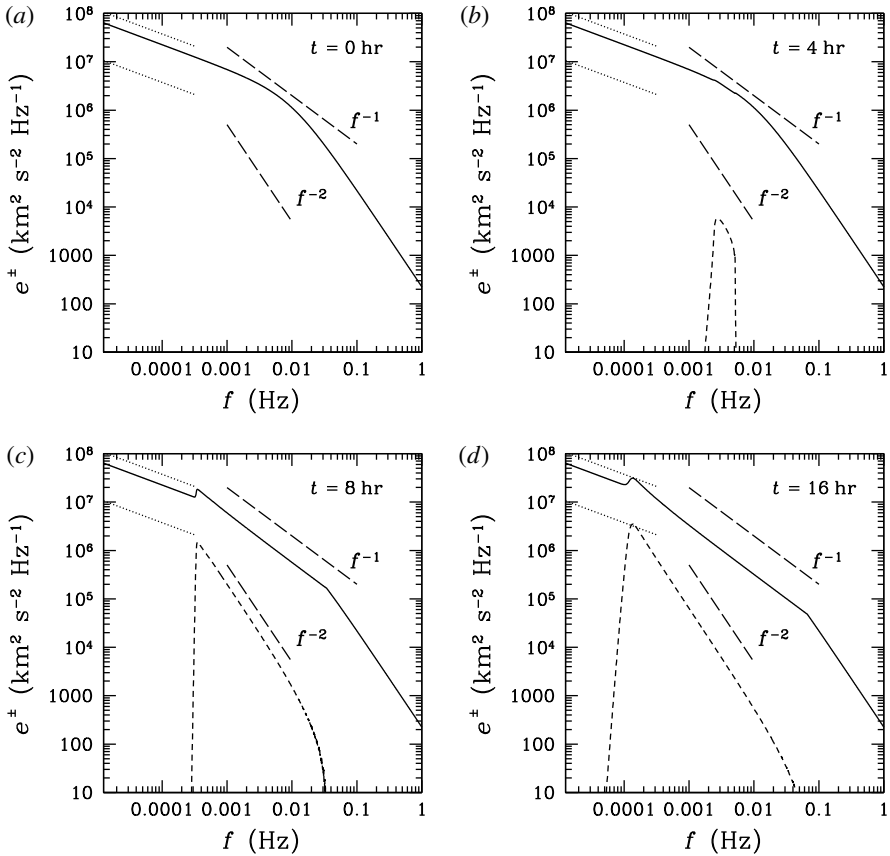
FIGURE 2. Solid lines show the AW power spectra in a numerical solution of (2.11) with plasma parameters and turbulence parameters chosen to model conditions in the fast solar wind at a heliocentric distance of 0.3 AU. The wavenumber spectra $E^{\pm}(k_z)$ appearing in (2.11) have been converted, using (6.3) and (6.4), into the frequency spectra $e^{\pm}(f)$. The dotted lines in the upper left corners of each plot show the evolutionary tracks of the values of e^+ and e^- at the low-frequency end of the frequency range in which $e^+ \propto f^{-1}$ in the approximate analytic solution to (2.11) presented in appendix B.

$(10^{-12}\sigma^+)$, so that the only source of dynamically important, inward-propagating AWs is the parametric decay of outward-propagating AWs.

Figure 2 summarizes the results of the calculation. Between $t = 0$ and $t = 4$ h, e^+ changes little while e^- grows rapidly between roughly 2 and 5 mHz, where the growth rate γ^- given in (3.1) peaks. Between $t = 4$ and $t = 8$ h, e^+ develops a broad $\sim 1/f$ scaling between $f = 3 \times 10^{-4}$ and $f = 3 \times 10^{-2}$ Hz, which shuts off the growth of e^- at these frequencies. At the same time, e^- acquires an $\sim f^{-2}$ scaling over much of this same frequency range. Between $t = 8$ and $t = 16$ h, the low-frequency limit of the $1/f$ range of e^+ decreases to $\sim 10^{-4}$ Hz, and the high-frequency limit of the $1/f$ range of e^+ increases to ~ 0.1 Hz.

The dotted lines in the upper left corner of each panel in figure 2 show the tracks followed by the values of e^+ and e^- at the low-frequency end of the frequency range in which $e^+ \propto f^{-1}$ in the approximate analytic solution to (2.11) that is described in appendix B. In this solution, E^+ and E^- are expanded in negative powers of k_z
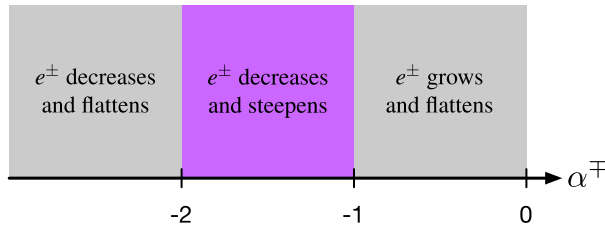
FIGURE 3. In this figure, it is assumed that the frequency spectra are initially power laws of the form $e^{\pm} \propto f^{\alpha^{\pm}}$, and that α^{+} and α^{-} are both negative. According to (6.11), parametric decay alters both the amplitude and slope of $e^{\pm}$ in the manner shown. For example, if $e^{-} \propto f^{-1.5}$, then $E^{+} \propto k_z^{-1.5}$, and (6.11) implies that E^{+} decreases at a rate that increases with k_z. This in turn implies that e^{+} decreases at a rate that increases with f, so that e^{+} steepens.
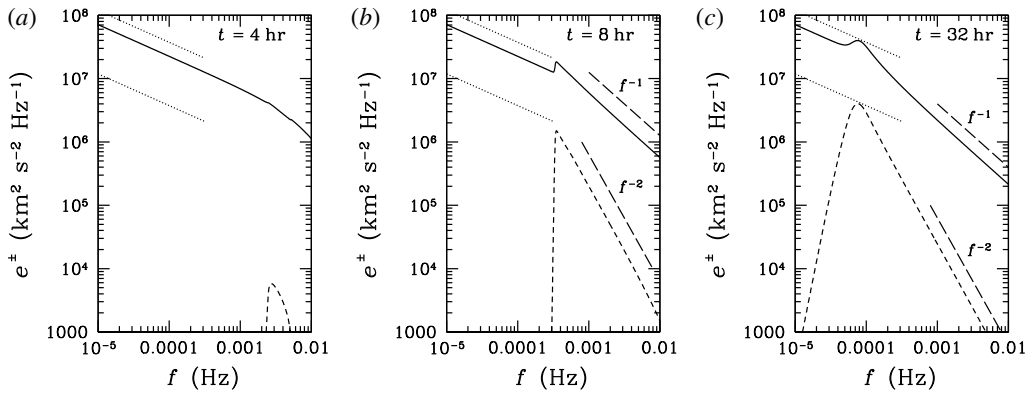

FIGURE 4. (*a,b*) Reproductions of the $t = 4$ and $t = 8$ h panels of figure 2 but with the axis ranges used in figure 2–2(*c*) of Tu & Marsch (1995). (*c*) From a later time ($t = 32$ h) in the same numerical solution.

at wavenumbers exceeding a time-dependent break wavenumber $b(t)$. Below this wavenumber, $E^{-} = 0$ and $E^{+} = \eta k_z^{p}$, where η and p are constants, and $-1 < p < 1$. At $k_z > b$, the dominant term in the expansion of E^{+} (E^{-}) scales like k_z^{-1} (k_z^{-2}), and the ratios of $E^{+}(b_+)$ to ηb_+^{p} and $E^{+}(b_+)$ to $E^{-}(b_+)$ are fixed functions of p, where b_+ is a wavenumber infinitesimally larger than b. For $p = -0.5$, $E^{+}(b_+)/\eta b_+^{p} = 5/3$ and $E^{+}(b_+)/E^{-}(b_+) = 10$, in approximate agreement with the numerical results (see also figure 4*c*).

6.1. *Heuristic explanation of the $e^{+} \propto f^{-1}$ and $e^{-} \propto f^{-2}$ scalings*

In order to understand the time evolution illustrated in figure 2, it is instructive to first consider the case in which

$$E^{\pm} = c^{\pm} k_z^{\alpha^{\pm}} \tag{6.10}$$

within some interval (k_{z1}, k_{z2}), where $c^{\pm}$ and $\alpha^{\pm}$ are constants. Equation (2.11) implies that, within this interval,

$$\frac{\partial}{\partial t} \ln E^{\pm} = \frac{\pi c^{\mp}}{v_A}(1 + \alpha^{\mp})k_z^{\alpha^{\mp}+2}. \tag{6.11}$$

If $\alpha^{\mp} > -1$, then $\ln E^{\pm}$ grows at a rate that increases with k_z, causing $E^{\pm}$ to increase and 'harden', in the sense that the best-fit value of $\alpha^{\pm}$ within the interval (k_{z1}, k_{z2}) increases. If $\alpha^{\mp} = -1$, then $E^{\pm}$ does not change. If $-2 < \alpha^{\mp} < -1$, then $\ln E^{\pm}$ decreases at a rate that increases with k_z, which causes the best-fit value of $\alpha^{\pm}$ within the interval (k_{z1}, k_{z2}) to decrease. If $\alpha^{\mp} = -2$, then $\ln E^{\pm}$ decreases at the same rate at all k_z, and $\alpha^{\pm}$ remains unchanged. Finally, if $\alpha^{\mp} < 2$, then $E^{\pm}$ decreases at a rate that decreases with k_z, which causes the best-fit value of $\alpha^{\pm}$ in the interval (k_{z1}, k_{z2}) to increase. These rules are summarized in figure 3 and apply to $e^{\pm} \propto f^{\alpha^{\pm}}$ as well as $E^{\pm} \propto k_z^{\alpha^{\pm}}$.

Returning to figure 2, in the early stages of the numerical calculation, e^{-} grows most rapidly at those frequencies at which γ^{-} in (3.1) is largest – namely, the high-f end of the $f^{-0.5}$ range of e^{+}. By the time e^{-} reaches a sufficient amplitude that e^{+} and e^{-} evolve on the same time scale, e^{-} develops a peaked frequency profile extending from some frequency $f = f_{\text{low}}$ to some larger frequency $f = f_{\text{high}}$, as illustrated in figure 2(b). Near f_{low}, $de^{-}/df > 0$ (i.e. $\alpha^{-} > 0$), which causes e^{+} to grow.[3] Near f_{high}, $\alpha^{-} < -1$, which causes e^{+} to decrease. Thus, e^{+} steepens across the interval $(f_{\text{low}}, f_{\text{high}})$ until it attains a $1/f$ scaling, at which point e^{-} stops growing between f_{low} and f_{high}. However, at frequencies just below f_{low}, e^{+} and e^{-} both continue to grow, causing f_{low} to decrease. At the same time, e^{+} continues to decrease at larger f where $\alpha^{-} < -1$. Together, the growth of e^{+} just below f_{low} and the damping of e^{+} at larger f cause the f^{-1} range of e^{+} to broaden in both directions, i.e. towards both smaller and larger frequencies.

The unique scaling of e^{-} consistent with an e^{+} spectrum $\propto f^{-1}$ that is a decreasing function of time is $e^{-} \propto f^{-2}$. Moreover, the scalings $e^{+} \sim f^{-1}$ and $e^{-} \sim f^{-2}$ are, in a sense, stable, as can be inferred from figure 3. For example, if α^{-} increases from -2 to a slightly larger value, then e^{+} decreases at a rate that increases with f, causing α^{+} to decrease to a value slightly below -1. This causes e^{-} to decrease at a rate that increases with f, thereby causing α^{-} to decrease back towards -2. A similar 'spectral restoring force' arises for any other small perturbation to the values $\alpha^{+} = -1$ and $\alpha^{-} = -2$.

It is worth emphasizing, in this context, that the analytic solution presented in appendix B is approximate rather than exact. As the spectral break frequency decreases past some fixed frequency f_3, the values of e^{+} and e^{-} at f_3 suddenly jump, but they do not jump to the precise values needed to extend the $e^{+} \sim f^{-1}$ and $e^{-} \sim f^{-2}$ scalings to smaller f. Instead, the spectra need further 'correcting' after the break frequency has swept past in order to maintain the scalings $e^{+} \sim f^{-1}$ and $e^{-} \sim f^{-2}$ in an approximate way. Also, the decrease in e^{-} that occurs after $t = 4$ h is a consequence of the sub-dominant f^{-2} component of e^{+}. This component of e^{+} becomes increasingly prominent near the break frequency as time progresses, leading to the pronounced curvature in the plot of e^{+} near $f = 10^{-4}$ Hz in figure 4(c).

6.2. *Comparison with Helios measurements*

In the (average) plasma rest frame, the equations of incompressible MHD can be written in the form

$$\frac{\partial z^{\pm}}{\partial t} + (z^{\mp} \pm v_{\text{A}}) \cdot \nabla z^{\pm} = -\nabla \Pi, \tag{6.12}$$

---

[3] Although the caption of figure 3 excludes positive $\alpha^{\mp}$ to allow use of the words 'flattens' and 'steepens' in the figure, equation (6.11) applies for positive $\alpha^{\mp}$.

where $z^{\pm} = \delta\boldsymbol{v} \mp \delta\boldsymbol{B}/\sqrt{4\pi\rho}$ are the Elsasser variables, $\delta\boldsymbol{v}$ and $\delta\boldsymbol{B}$ are the velocity and magnetic-field fluctuations, ρ is the mass density, $\boldsymbol{v}_{\mathrm{A}} = \boldsymbol{B}_0/\sqrt{4\pi\rho}$ is the Alfvén velocity and Π is the total pressure divided by ρ (Elsasser 1950). Although the solar wind is compressible, equation (6.12) provides a reasonable approximation for the non-compressive, AW-like component of solar-wind turbulence. As (6.12) shows, the advection velocity of a $z^{\pm}$ fluctuation is $z^{\mp} \pm \boldsymbol{v}_{\mathrm{A}}$. This implies, as shown by Maron & Goldreich (2001), that $z^{\pm}$ fluctuations propagate along magnetic field lines perturbed by $z^{\mp}$. As a consequence, in the solar wind, when the root-mean-square (rms) magnetic-field fluctuation δB_{in} associated with inward-propagating AWs (z^{-}) is much smaller than the background magnetic field B_0, the outward-propagating AWs (z^{+}) propagate to a good approximation along the direction of $\boldsymbol{B}_0$. This is true even if the rms magnetic-field fluctuation δB_{out} associated with z^{+} is comparable to B_0. In the fast solar wind at $r < 0.3$ AU, the (fractional) cross-helicity is high (i.e. $E^{+} \gg E^{-}$), and δB_{in} is indeed small compared to B_0 (Bavassano, Pietropaolo & Bruno 2000; Cranmer & van Ballegooijen 2005). Moreover, the background magnetic field at $r = 0.3$ AU is nearly in the radial direction, because the Parker-spiral magnetic field begins to deviate appreciably from the radial direction only at larger r in the fast wind (Verscharen *et al.* 2015). Hence, in high-cross-helicity fast-wind streams at $r = 0.3$ AU, the function e^{+} defined by (6.3) and (6.4) corresponds to a good approximation to the frequency spectrum of outward-propagating AWs observed by a spacecraft in the solar wind. It is not clear, however, how well e^{-} corresponds to the observed spectrum of inward-propagating AWs, because the inward-propagating AWs follow field lines perturbed by the outward-propagating AWs, which can be inclined relative to the radial direction by a substantial angle.

Figure 4 reproduces the $t = 4$ h and $t = 8$ h panels of figure 2, but with the same axis ranges as those in figure 2–2(*c*) of Tu & Marsch (1995) to facilitate comparison. Figure 4 also includes a third panel that shows the spectra at $t = 32$ h. The e^{+} spectrum in the $t = 8$ h panel of figure 2 shares a number of properties with the e^{+} spectrum in figure 2–2(*c*) of Tu & Marsch (1995), in addition to the $f^{-0.5}$ scaling at small f that was built in to the numerical calculation as an initial condition. In particular, $e^{+} \gg e^{-}$ at all frequencies, $e^{+} \sim f^{-1}$ at $f \gtrsim 3 \times 10^{-4}$ Hz, and there is a bump in the e^{+} spectrum at the transition between the $f^{-0.5}$ and f^{-1} scaling ranges of e^{+}.

Although this comparison is suggestive, it is not entirely clear how to map time in the numerical calculation to heliocentric distance in the solar wind, because the plasma parameters in the numerical calculation are independent of position and time, whereas they depend strongly upon heliocentric distance in the solar wind. For example, the turbulence is weaker (in the sense of smaller $\delta v_0/v_{\mathrm{A}}$) the closer one gets to the Sun. (See also the discussion following (7.10).) Also, the choice of initial conditions in the numerical calculation artificially prolongs the linear stage of evolution, since in the solar wind there are sources of inward-propagating waves other than parametric instability, such as non-WKB reflection (Heinemann & Olbert 1980; Velli 1993). Nevertheless, as a baseline for comparison, the travel time of an outward-propagating AW from the photosphere to 0.3 AU in the fast-solar-wind model developed by Chandran & Hollweg (2009) is approximately 12 h.

7. Discussion of approximations and relevance to the solar wind

This section critically assesses the assumptions underlying the results in §§ 2 through 6 and the degree to which these assumptions apply to the fast solar wind between $r = 10R_{\odot}$ (the approximate perihelion of the Parker Solar Probe) and $r = 0.3$ AU.

7.1. *The weak-turbulence approximation*

A central assumption of the analysis is the weak-turbulence criterion in (2.1). Since E^+ and E^- differ in the solar wind, equation (2.1) is really two conditions,

$$\omega_{\mathrm{nl}}^{\pm} \ll |k_z| v_{\mathrm{A}}, \tag{7.1}$$

where ω_{nl}^{+} (ω_{nl}^{-}) is the inverse of the time scale on which nonlinear interactions modify outward-propagating (inward-propagating) AWs. The contribution to $\omega_{\mathrm{nl}}^{\pm}$ from the parametric instability is

$$\omega_{\mathrm{nl,PI}}^{\pm} \sim \frac{1}{E^{\pm}} \left| \frac{\partial E^{\pm}}{\partial t} \right| \sim \frac{k_z^2 E^{\mp}}{v_{\mathrm{A}}}. \tag{7.2}$$

The contribution to $\omega_{\mathrm{nl}}^{\pm}$ from one other type of nonlinear interaction is estimated in § 7.3. The estimate of $\partial E^{\pm}/\partial t$ in (7.2) follows from (2.11) and setting $E^{\mp} \sim |k_z|^{\alpha^{\mp}}$ with $\alpha^{\mp}$ not very close to -1. An approximate upper limit on $\omega_{\mathrm{nl,PI}}^{\pm}$ results from replacing $k_z E^{\mp}$ in (7.2) with $(\delta v^{\mp})^2$, where $(\delta v^+)^2$ is the mean-square velocity fluctuation associated with outward-propagating AWs, and $(\delta v^-)^2$ is the mean-square velocity fluctuation associated with inward-propagating AWs. This leads to an approximate upper limit on $\omega_{\mathrm{nl,PI}}^{\pm}$ because $(\delta v^{\pm})^2$ includes contributions from all wavenumbers and is much larger than the value of $k_z E^{\pm}$ at some k_z. Equation (7.1), with $\omega_{\mathrm{nl}} \sim \omega_{\mathrm{nl,PI}}$, is thus satisfied provided

$$(\delta v^{\mp})^2 \ll v_{\mathrm{A}}^2. \tag{7.3}$$

Bavassano *et al.* (2000) analysed *Helios* measurements of fluctuations in the fast solar wind at $r = 0.4$ AU and found that $(\delta v^-)^2 \ll (\delta v^+)^2 \simeq (60 \text{ km s}^{-1})^2$. As mentioned above, the typical value of v_{A} in the fast solar wind at $r = 0.3$ AU is $\sim 150 \text{ km s}^{-1}$ (Marsch *et al.* 1982; Marsch & Tu 1990). Near $r = 0.3$ AU, $B_0 \sim 1/r^2$, $\rho \sim 1/r^2$ and $v_{\mathrm{A}} \sim 1/r$, and so the typical value of v_{A} in fast-solar-wind streams at $r = 0.4$ AU is $\sim 112.5 \text{ km s}^{-1}$. These measurements indicate that

$$(\delta v^-)^2 \ll (\delta v^+)^2 \simeq 0.28 v_{\mathrm{A}}^2 \tag{7.4}$$

in the fast solar wind at $r = 0.4$ AU. Since $\delta v^{\pm}/v_{\mathrm{A}}$ decreases as r decreases below 0.4 AU (Cranmer & van Ballegooijen 2005; Chandran & Hollweg 2009), the condition $\omega_{\mathrm{nl,PI}}^{+} \ll |k_z| v_{\mathrm{A}}$ is well satisfied at $r < 0.4$ AU, and the condition $\omega_{\mathrm{nl,PI}}^{-} \ll |k_z| v_{\mathrm{A}}$ is at least marginally satisfied at $r < 0.4$ AU.

It is worth noting that weak-turbulence theory fails when applied to resonant interactions between three AWs, because such interactions occur only when one of the AWs has zero frequency, violating the weak-turbulence ordering (Schekochihin, Nazarenko & Yousef 2012; Meyrand, Kiyani & Galtier 2015). In contrast, the AW/slow-wave interactions in parametric decay do not involve a zero-frequency mode. Weak-turbulence theory is thus in principle a better approximation for the nonlinear evolution of the parametric instability than for incompressible MHD turbulence.

7.2. *The low-β assumption*

The assumption that $\beta \ll 1$ is not satisfied at $r \gtrsim 0.3 \text{ AU} \simeq 65 R_{\odot}$, where β is typically ~ 1, but is reasonable at $r \lesssim 20 R_{\odot}$ (Chandran *et al.* 2011). It is possible that the $\beta \ll 1$ theory presented here applies at least at a qualitative level provided β is simply $\lesssim 1$, and indeed this possibility motivates the comparison of the present model with *Helios* observations. However, further work is needed to investigate how the results of this paper are modified as β increases to values ~ 1.

7.3. *Neglect of other types of nonlinear interactions*

Another approximation in §§ 2 through 6 is the neglect of all nonlinear interactions besides parametric decay. One of the neglected interactions is the shearing of inward-propagating AWs by outward-propagating AWs, which makes a contribution to ω_{nl}^{-} that depends on the perpendicular length scale of the AWs. At the perpendicular outer scale $L_{\perp}$ (the overall correlation length of the AWs measured perpendicular to $\boldsymbol{B}_0$), the contribution to ω_{nl}^{-} from shearing is approximately

$$\omega_{nl,\perp}^{-} \sim \frac{\chi \delta v^{+}}{L_{\perp}}, \tag{7.5}$$

where

$$\chi = \frac{\delta v^{+}}{k_z L_{\perp} v_A} \tag{7.6}$$

is the critical-balance parameter (Goldreich & Sridhar 1995; Ng & Bhattacharjee 1996; Lithwick, Goldreich & Sridhar 2007). Equation (7.5) does not apply when χ is much larger than 1, but direct numerical simulations suggest that $\chi \lesssim 1$ at $r \gtrsim 10R_{\odot}$ for the bulk of the AW energy (J. Perez, private communication). Thus, at $r \gtrsim 10R_{\odot}$,

$$\frac{\omega_{nl,PI}^{-}}{\omega_{nl,\perp}^{-}} \simeq (k_z L_{\perp})^2. \tag{7.7}$$

As AWs propagate away from the Sun, they follow magnetic field lines, which leads to the approximate scaling $L_{\perp} \propto B_0^{-1/2}$. In the WKB limit, the AW frequency in the Sun's frame $k_z(U + v_A)$ is independent of r. The scaling $k_z \sim 1/(U + v_A)$ thus serves as a rough approximation for outward-propagating AWs in the turbulent solar wind. At the coronal base (just above the transition region), where k_z and $L_{\perp}$ have the values k_{zb} and $L_{\perp b}$, the value of $k_{zb}L_{\perp b}$ for the energetically dominant AWs launched by the Sun can be estimated (in essence from the critical-balance condition) as $\delta v_b^+/v_{Ab}$, where δv_b^+ and v_{Ab} are the values of δv^+ and v_A at the coronal base (Goldreich & Sridhar 1995; van Ballegooijen & Asgari-Targhi 2016). Together, these scalings lead to the estimate

$$k_z L_{\perp} \simeq \sqrt{\frac{B_{0b}}{B_0}} \left(\frac{U_b + v_{Ab}}{U + v_A} \right) \frac{\delta v_b^+}{v_{Ab}}, \tag{7.8}$$

where B_{0b} and U_b are the values of the background magnetic field and solar-wind outflow velocity at the coronal base. Between $r = 10R_{\odot}$ and $r = 60R_{\odot}$, $B_{0b}/B_0 \simeq f_{max}(r/R_{\odot})^2$, where f_{max} is the super-radial expansion factor (Kopp & Holzer 1976). In the fast solar wind within this range of radii, $U + v_A \simeq 700$–800 km s^{-1}, which is comparable to $U_b + v_{Ab} \simeq v_{Ab} \simeq 10^3$ km s^{-1}. Equation (7.8) is thus approximately equivalent to

$$k_z L_{\perp} \simeq \sqrt{f_{max}} \left(\frac{r}{R_{\odot}} \right) \left(\frac{\delta v_b^+}{v_{Ab}} \right) \tag{7.9}$$

for the energetically dominant fluctuations launched by the Sun. If we set $f_{max} = 9$, $\delta v_b = 30$ km s^{-1}, and $v_{Ab} = 900$ km s^{-1}, then (7.9) becomes

$$k_z L_{\perp} \sim \frac{r}{10R_{\odot}} \tag{7.10}$$

for the energetically dominant AWs launched by the Sun. Equations (7.7) and (7.10) suggest that it is reasonable to neglect the shearing of inward-propagating AWs by outward-propagating AWs at $r \gtrsim 10R_\odot$. On the other hand, at smaller radii, shearing could suppress the growth of inward-propagating AWs that would otherwise result from the parametric instability. Also, the requirement that $k_z L_\perp > 1$ in order for $\omega_{\mathrm{nl,PI}}^-$ to exceed $\omega_{\mathrm{nl},\perp}^-$ could prevent the f^{-1} range from spreading to frequencies below some minimum (r-dependent) value.

The other nonlinearities in the weak-turbulence wave kinetic equations that are neglected in this paper include interactions involving fast magnetosonic waves, the turbulent mixing of slow waves by AWs, phase mixing of AWs by slow waves and the shearing of outward-propagating AWs by inward-propagating AWs (Chandran 2008). *In situ* measurements indicate that fast waves account for only a small fraction of the energy in compressive fluctuations at 1 AU (Yao *et al.* 2011; Howes *et al.* 2012; Klein *et al.* 2012). Also, fast waves propagating away from the Sun undergo almost complete reflection before they can escape into the corona (Hollweg 1978). These findings suggest that nonlinear interactions involving fast waves have little effect upon the conclusions of this paper. The turbulent mixing of slow waves by AWs acts as an additional slow-wave damping mechanism and is thus unlikely to change the conclusions of this paper, which already assume strong slow-wave damping. Phase mixing of AWs by slow waves transports AW energy to larger $k_\perp$ at a rate that increases with $|k_z|$ (Chandran 2008). Although the fractional density fluctuations between $r = 10R_\odot$ and $r = 0.3$ AU are fairly small (see, e.g. Tu & Marsch 1995; Hollweg *et al.* 2010), phase mixing could affect the parallel AW power spectra, and further work is needed to investigate this possibility. The shearing of outward-propagating AWs by inward-propagating AWs is enhanced by non-WKB reflection, which makes this shearing more coherent in time (Velli *et al.* 1989). The resulting nonlinear time scale for outward-propagating AWs is approximately $r/(U + v_A)$ (Chandran & Hollweg 2009), where U is the solar-wind outflow velocity. This time scale is comparable to the AW propagation time from the Sun to heliocentric distance r, and hence to the parametric-decay time scale at the small-f end of the $1/f$ range of e^+. How this shearing modifies $E^+(k_z)$, however, is not clear. For example, shearing by inward-propagating AWs may transport outward-propagating-AW energy to larger $k_\perp = \sqrt{k_x^2 + k_y^2}$ at a rate that is independent of $|k_z|$, in which case this shearing would reduce $E^+(k_z)$ by approximately the same factor at all k_z, leaving the functional form of $E^+(k_z)$ unchanged.

7.4. *Neglect of spatial inhomogeneity*

In this paper, it is assumed that the background plasma is uniform and stationary. In the solar wind, however, as an AW propagates from the low corona to 0.3 AU, the properties of the ambient plasma seen by the AW change dramatically, with β increasing from $\sim 10^{-2}$ to ~ 1 and $\delta v_{\mathrm{rms}}/v_A$ increasing from ~ 0.02 to ~ 0.5 (Bavassano *et al.* 2000; Cranmer & van Ballegooijen 2005; Chandran *et al.* 2011). Further work is needed to determine how this spatial inhomogeneity affects the nonlinear evolution of the parametric instability.

7.5. *Approximate treatment of slow-wave damping*

A key assumption in §§ 2 through 6 is that slow waves are strongly damped, and this damping is implemented by neglecting terms in the wave kinetic equations that are

proportional to the slow-wave power spectrum $S_k^{\pm}$. There are two sources of error in this approach. First, damping could modify the polarization properties of slow waves, thereby altering the wave kinetic equations. Second, even if $S_k^{\pm}$ is much smaller than the AW power spectrum $A_k^{\pm}$, the neglected parametric-decay terms in the wave kinetic equations for AWs that are proportional to $S_k^{\pm}$ could still be important, because they contain a factor of β^{-1}, which is absent in the terms that are retained. This factor arises from the fact that the fractional density fluctuation of a slow wave is $\sim \beta^{-1/2}$ times larger than the fractional magnetic-field fluctuation of an AW with equal energy. These neglected terms act to equalize the 3-D AW power spectra A^+ and A^-, and hence to equalize E^+ and E^-. If these neglected terms were in fact important, they could invalidate the solutions presented in §6, in which $E^+ \gg E^-$. However, *in situ* observations indicate that $E^+ \gg E^-$ in the fast solar wind at $r = 0.3$ AU (Marsch & Tu 1990; Tu & Marsch 1995), which suggests that the neglect of these terms is reasonable. Further work is needed to investigate these issues more carefully.

8. Conclusion

In this paper, weak-turbulence theory is used to investigate the nonlinear evolution of the parametric instability in low-β plasmas. The analysis starts from the wave kinetic equations describing the interactions between AWs and slow waves in weak compressible MHD turbulence. To account for the strong damping of slow waves in collisionless plasmas, terms containing the slow-wave energy density are dropped. The equations allow for all wave-vector directions, but are integrated over the wave-vector components perpendicular to the background magnetic field $\boldsymbol{B}_0$ (k_x and k_y), which leads to equations for the 1-D power spectra E^+ and E^- that depend only on the parallel wavenumber k_z and time. During parametric decay in a low-β plasma, an AW decays into a slow-wave propagating in the same direction and a counter-propagating AW with a frequency slightly smaller than the frequency of the initial AW. The total number of AW quanta is conserved, and the reduction in AW frequencies leads to an inverse cascade of AW quanta towards smaller ω and k_z. The energy of each AW quantum is $\hbar\omega$, and the decrease in ω during each decay corresponds to a decrease in the AW energy, which is compensated for by an increase in the slow-wave energy. The subsequent damping and dissipation of slow-wave energy results in plasma heating.

The main results of this paper concern the parametric decay of a population of AWs propagating in one direction, say parallel to $\boldsymbol{B}_0$, when the counter-propagating AWs start out with much smaller amplitudes. If the initial frequency spectrum e^+ of the parallel-propagating AWs has a peak frequency f_0 (at which fe^+ is maximized) and an 'infrared' scaling f^p at smaller f with $-1 < p < 1$, then e^+ acquires a $1/f$ scaling throughout a range of frequencies that spreads out in both directions from f_0. At the same time, the anti-parallel-propagating AWs acquire a $1/f^2$ spectrum within this same frequency range. If the plasma parameters and infrared e^+ spectrum are chosen to match conditions in the fast solar wind at a heliocentric distance of 0.3 AU, and the AWs are allowed to evolve for a period of time that is approximately two thirds of the AW travel time from the Sun to 0.3 AU, the resulting form of e^+ is similar to the form observed by the *Helios* spacecraft in the fast solar wind at 0.3 AU. Because the background plasma parameters are time independent in the analysis of this paper but time dependent in the plasma rest frame in the solar wind, it is not clear how to map the time variable in the present analysis to heliocentric distance. Nevertheless, the similarity between the spectra found in this paper and the spectra observed by *Helios* suggests that parametric decay plays an important role in shaping the AW spectra observed in the fast solar wind at 0.3 AU, at least for wave periods $\lesssim 1$ h.

The frequency f^* that dominates the AW energy is the maximum of $(fe^+ + fe^-)$. At the beginning of the numerical calculation presented in §6, f^* is approximately $f_0 = 0.01$ Hz. At $t = 8$ h in this numerical calculation, f^* is the smallest frequency at which $e^+ \sim f^{-1}$ and $e^- \sim f^{-2}$, which is $\sim 3 \times 10^{-4}$ Hz. This decrease in f^* is a consequence of the aforementioned inverse cascade, which transports AW quanta from the initial peak frequency to smaller frequencies. Inverse cascade offers a way to reconcile the observed dominance of AWs at hour-long time scales at 0.3 AU with arguments that the Sun launches most of its AW power at significantly shorter wave periods (Cranmer & van Ballegooijen 2005; van Ballegooijen & Asgari-Targhi 2016).

Further work is needed to relax some of the simplifying assumptions in this paper, including the low-β approximation, the assumption of spatial homogeneity, the simplistic treatment of slow-wave damping, and the neglect of nonlinear interactions other than parametric decay. Further work is also needed to evaluate the relative contributions of parametric decay and other mechanisms to the generation of $1/f$ spectra in the solar wind. For example, Matthaeus & Goldstein (1986) argued that the f^{-1} spectrum seen at $r = 1$ AU at $3 \times 10^{-6} < f < 8 \times 10^{-5}$ Hz is a consequence of forcing at the solar surface, and Velli *et al.* (1989) argued that the shearing of outward-propagating AWs by the inward-propagating AWs produced by non-WKB reflection causes the outward-propagating AWs to acquire an f^{-1} spectrum.

NASA's Parker Solar Probe (PSP) has a planned launch date in the summer of 2018 and will reach heliocentric distances less than $10R_\odot$. The FIELDS (Bale *et al.* 2016) and SWEAP (Kasper *et al.* 2015) instrument suites on PSP will provide the first ever *in situ* measurements of the magnetic-field, electric-field, velocity and density fluctuations in the solar wind at $r < 0.29$ AU. Although the issues mentioned in the preceding paragraph are sources of uncertainty, the results of this paper lead to the following predictions that will be tested by PSP. First, the $1/f$ range of e^+ in fast-solar-wind streams at $r < 0.3$ AU and $f \gtrsim 3 \times 10^{-4}$ Hz is produced *in situ* by parametric decay. As a consequence, the $1/f$ range of e^+ in fast-solar-wind streams will be much more narrow at small r than at $r = 0.3$ AU. As AWs propagate away from the Sun, the frequency range $(f_{\min}, f_{\max})$ in which $e^+ \sim 1/f$ spreads out in both directions from the near-Sun peak frequency (the maximum of fe^+). Thus, $f_{\min}$ will be larger closer to the Sun, and $f_{\max}$ will be smaller. Finally, during epochs in which the local magnetic field is aligned with the relative velocity between the plasma and the spacecraft (see the discussion in §6.2), the spectrum of e^- will scale like $1/f^2$ in the frequency interval $(f_{\min}, f_{\max})$.

Appendix A. Boundary layers in the Alfvén-wave power spectra

In this appendix, a small nonlinear diffusion term is added to the wave kinetic equation, so that (2.11) becomes

$$\frac{\partial E^\pm}{\partial t} = \frac{\pi}{v_A} k_z^2 E^\pm \frac{\partial}{\partial k_z}(k_z E^\mp) + \nu \overline{E^\mp} \frac{\partial^2}{\partial k_z^2} E^\pm, \tag{A 1}$$

where ν is a constant that is taken to be very small,

$$\overline{E^{\mp}}(k_z, t) = \frac{1}{2\Delta} \int_{k_z-\Delta}^{k_z+\Delta} E^{\mp} \, dk_z, \tag{A 2}$$

and Δ is a wavenumber increment that is $\ll |k_z|$ but which remains finite as $\nu \to 0$. A solution to (A 1) is sought in which $E^{\pm}$ has a boundary layer at some wavenumber $k_z = b(t)$. For simplicity, the analysis is restricted to $k_z > 0$. The spectra at negative k_z values then follow from the fact that E^+ and E^- are even functions of k_z.

It is useful to work with the dimensionless variables defined through the equations

$$k_z = sk_{z0}, \quad t = \tau \left[\frac{v_A}{\pi k_{z0}(\delta v_0)^2} \right], \quad E^{\pm} = \frac{\tilde{E}^{\pm}(\delta v_0)^2}{k_{z0}}, \quad \overline{E^{\pm}} = \frac{\overline{\tilde{E}^{\pm}}(\delta v_0)^2}{k_{z0}}, \tag{A 3a--d}$$

where k_{z0} is some characteristic wavenumber and $(\delta v_0)^2$ is the characteristic mean-square AW velocity fluctuation. The analysis is restricted to the case in which

$$H \equiv \tilde{E}^+ = \tilde{E}^-. \tag{A 4}$$

Equation (A 1) then takes the form

$$\frac{\partial H}{\partial \tau} = s^2 H \frac{\partial}{\partial s}(sH) + \epsilon \overline{H} \frac{\partial^2 H}{\partial s^2}, \tag{A 5}$$

where $\overline{H} = \overline{\tilde{E}^+}$ and

$$\epsilon = \frac{\nu v_A}{\pi k_{z0}^4} \ll 1. \tag{A 6}$$

Upon setting $H = H(x, \tau)$ in (A 5), where

$$\epsilon x = s - \tilde{b}, \quad \tilde{b} = \frac{b}{k_{z0}}, \tag{A 7a,b}$$

and discarding terms $\ll \epsilon^{-1}$, one obtains

$$0 = \left(\frac{d\tilde{b}}{d\tau} + \tilde{b}^3 H \right) \frac{\partial H}{\partial x} + \overline{H} \frac{\partial^2 H}{\partial x^2}, \tag{A 8}$$

where $\overline{H}$ is independent of x.

As in (5.1) and (5.8), it is assumed that $H = 0$ on the small-k_z side of the boundary layer at $s = \tilde{b}$. The value of H at dimensionless wavenumbers slightly larger than $\tilde{b}$ is denoted $H_>$. The solution to (A 8) must thus satisfy the boundary conditions

$$H \to \begin{cases} 0 & \text{as } x \to -\infty, \\ H_> & \text{as } x \to \infty, \end{cases} \tag{A 9}$$

with $\overline{H} = H_>/2$. Upon substituting

$$H = \frac{H_>}{2} \left(1 + \tanh \frac{x}{a} \right) \tag{A 10}$$

into (A 8), one finds that

$$0 = \left(\frac{d\tilde{b}}{d\tau} \right) \frac{H_>}{2a} \operatorname{sech}^2 \left(\frac{x}{a} \right) + \frac{H_>^2 \tilde{b}^3}{4a} \left(1 + \tanh \frac{x}{a} \right) \operatorname{sech}^2 \left(\frac{x}{a} \right) - \frac{H_>^2}{2a^2} \operatorname{sech}^2 \left(\frac{x}{a} \right) \tanh \frac{x}{a}. \tag{A 11}$$

By separately equating the $\operatorname{sech}^2(x/a)$ terms and the $\tanh(x/a)\operatorname{sech}^2(x/a)$ terms, one obtains

$$\frac{d\tilde{b}}{d\tau} = -\frac{H_> \tilde{b}^3}{2} \tag{A 12}$$

and

$$a = \frac{2}{\tilde{b}^3}. \tag{A 13}$$

Thus, the desired solution to (A 8) is (A 10) with a and $\tilde{b}$ given by (A 12) and (A 13). Equation (A 12) can be rewritten in terms of the original variables as

$$\frac{db}{dt} = -\frac{\pi b^3 E_>}{2v_A}, \tag{A 14}$$

where $E_> = H_>(\delta v_0)^2/k_{z0}$, which is equivalent to (5.4).

Appendix B. Approximate analytic solution for decaying, cross-helical Alfvén waves in the nonlinear regime

In this appendix, a solution to (2.11) is sought in which

$$E^+ = H(k_z - b) \sum_{n=1}^{\infty} c_n \left(\frac{k_z}{b} \right)^{-n} + H(b - k_z) \eta k_z^p, \tag{B 1}$$

$$E^- = H(k_z - b) \sum_{n=2}^{\infty} a_n \left(\frac{k_z}{b} \right)^{-n}, \tag{B 2}$$

and

$$c_{n+1} \ll c_n \quad a_{n+1} \ll a_n \quad a_2 \ll c_1, \tag{B 3}$$

where $H(x)$ is the Heaviside function, a_n, b and c_n are functions of time, and η and p are constants, with

$$-1 < p < 1. \tag{B 4}$$

Substituting (B 1) and (B 2) into (2.11) and making use of (B 3) leads to the following approximate solutions for b, c_1 and a_2:

$$b = \left[\frac{(p+2)(p+1)\pi\eta t}{(1-p)v_A} + \Lambda \right]^{-1/(p+2)}, \tag{B 5}$$

where Λ is a constant of integration,

$$c_1 = \frac{(p+3)\eta b^p}{1-p}, \tag{B 6}$$

and

$$a_2 = \frac{(p+1)^2 \eta b^p}{1-p}. \tag{B 7}$$

Equations (B 5) through (B 7) imply that the break wavenumber $b(t)$ decreases in time, and that the ratios $E^+(b_+)/\eta b_+^p$ and $E^+(b_+)/E^-(b_+)$ remain constant, where b_+ is a wavenumber infinitesimally larger than b. For example, if the infrared spectral index p is $-1/2$, then

$$\frac{E^+(b_+)}{E^-(b_+)} = \frac{p+3}{(p+1)^2} \to 10, \tag{B 8}$$

and

$$\frac{E^+(b_+)}{\eta b_+^p} = \frac{p+3}{1-p} \to \frac{5}{3}. \tag{B 9}$$

Equations (B 8) and (B 9) are shown as dotted lines in figures 2 and 4.

REFERENCES

ARANEDA, J. A., MARSCH, E. & VIÑAS, A. F. 2008 Proton core heating and beam formation via parametrically unstable Alfvén-cyclotron waves. *Phys. Rev. Lett.* **100** (12), 125003.

BALE, S. D., GOETZ, K., HARVEY, P. R., TURIN, P., BONNELL, J. W., DUDOK DE WIT, T., ERGUN, R. E., MACDOWALL, R. J., PULUPA, M., ANDRE, M. *et al.* 2016 The FIELDS instrument suite for solar probe plus. Measuring the coronal plasma and magnetic field, plasma waves and turbulence, and radio signatures of solar transients. *Space Sci. Rev.* **204**, 49–82.

VAN BALLEGOOIJEN, A. A. & ASGARI-TARGHI, M. 2016 Heating and acceleration of the fast solar wind by Alfvén wave turbulence. *Astrophys. J.* **821**, 106.

VAN BALLEGOOIJEN, A. A. & ASGARI-TARGHI, M. 2017 Direct and inverse cascades in the acceleration region of the fast solar wind. *Astrophys. J.* **835**, 10.

BARNES, A. 1966 Collisionless damping of hydromagnetic waves. *Phys. Fluids* **9**, 1483–1495.

BAVASSANO, B., PIETROPAOLO, E. & BRUNO, R. 2000 On the evolution of outward and inward Alfvénic fluctuations in the polar wind. *J. Geophys. Res.* **105**, 15959–15964.

CHANDRAN, B. D. G. 2008 Weakly turbulent magnetohydrodynamic waves in compressible low-β plasmas. *Phys. Rev. Lett.* **101** (23), 235004.

CHANDRAN, B. D. G., DENNIS, T. J., QUATAERT, E. & BALE, S. D. 2011 Incorporating kinetic physics into a two-fluid solar-wind model with temperature anisotropy and low-frequency Alfvén-wave turbulence. *Astrophys. J.* **743**, 197.

CHANDRAN, B. D. G. & HOLLWEG, J. V. 2009 Alfvén wave reflection and turbulent heating in the solar wind from 1 solar radius to 1 AU: an analytical treatment. *Astrophys. J.* **707**, 1659–1667.

COHEN, R. H. & DEWAR, R. L. 1974 On the backscatter instability of solar wind Alfven waves. *J. Geophys. Res.* **79**, 4174–4178.

CRANMER, S. R. & VAN BALLEGOOIJEN, A. A. 2005 On the generation, propagation, and reflection of Alfvén waves from the solar photosphere to the distant heliosphere. *Astrophys. J. Suppl.* **156**, 265–293.

CRANMER, S. R., VAN BALLEGOOIJEN, A. A. & EDGAR, R. J. 2007 Self-consistent coronal heating and solar wind acceleration from anisotropic magnetohydrodynamic turbulence. *Astrophys. J. Suppl.* **171**, 520–551.

DEL ZANNA, L., VELLI, M. & LONDRILLO, P. 2001 Parametric decay of circularly polarized Alfvén waves: multidimensional simulations in periodic and open domains. *Astron. Astrophys.* **367**, 705–718.

DOBROWOLNY, M., MANGENEY, A. & VELTRI, P. 1980 Fully developed anisotropic hydromagnetic turbulence in interplanetary space. *Phys. Rev. Lett.* **45**, 144–147.

DORFMAN, S. & CARTER, T. A. 2016 Observation of an Alfvén wave parametric instability in a laboratory plasma. *Phys. Rev. Lett.* **116** (19), 195002.

ELSASSER, W. M. 1950 The hydromagnetic equations. *Phys. Rev.* **79**, 183.

FORMAN, M. A., WICKS, R. T. & HORBURY, T. S. 2011 Detailed fit of 'Critical Balance' theory to solar wind turbulence measurements. *Astrophys. J.* **733**, 76.

GALEEV, A. A. & ORAEVSKII, V. N. 1963 The stability of Alfvén waves. *Sov. Phys. Dokl.* **7**, 988.

GALTIER, S., NAZARENKO, S. V., NEWELL, A. C. & POUQUET, A. 2000 A weak turbulence theory for incompressible magnetohydrodynamics. *J. Plasma Phys.* **63**, 447–488.

GOLDREICH, P. & SRIDHAR, S. 1995 Toward a theory of interstellar turbulence. 2: strong Alfvenic turbulence. *Astrophys. J.* **438**, 763–775.

GOLDSTEIN, M. L. 1978 An instability of finite amplitude circularly polarized Alfven waves. *Astrophys. J.* **219**, 700–704.

HEINEMANN, M. & OLBERT, S. 1980 Non-WKB Alfven waves in the solar wind. *J. Geophys. Res.* **85**, 1311–1327.

HEYVAERTS, J. & PRIEST, E. R. 1983 Coronal heating by phase-mixed shear Alfven waves. *Astron. Astrophys.* **117**, 220–234.

HOLLWEG, J. V. 1978 Fast wave evanescence in the solar corona. *Geophys. Res. Lett.* **5**, 731–734.

HOLLWEG, J. V. 1994 Beat, modulational, and decay instabilities of a circularly polarized Alfven wave. *J. Geophys. Res.* **99**, 23.

HOLLWEG, J. V., CRANMER, S. R. & CHANDRAN, B. D. G. 2010 Coronal Faraday rotation fluctuations and a wave/turbulence-driven model of the solar wind. *Astrophys. J.* **722**, 1495–1503.

VAN DER HOLST, B., SOKOLOV, I. V., MENG, X., JIN, M., MANCHESTER IV, W. B., TÓTH, G. & GOMBOSI, T. I. 2014 Alfvén wave solar model (AWSoM): coronal heating. *Astrophys. J.* **782**, 81.

HORBURY, T. S., FORMAN, M. & OUGHTON, S. 2008 Anisotropic scaling of magnetohydrodynamic turbulence. *Phys. Rev. Lett.* **101** (17), 175005.

HOWES, G. G., BALE, S. D., KLEIN, K. G., CHEN, C. H. K., SALEM, C. S. & TENBARGE, J. M. 2012 The slow-mode nature of compressible wave power in solar wind turbulence. *Astrophys. J. Lett.* **753**, L19.

INHESTER, B. 1990 A drift-kinetic treatment of the parametric decay of large-amplitude Alfven waves. *J. Geophys. Res.* **95**, 10525–10539.

KASPER, J. C., ABIAD, R., AUSTIN, G., BALAT-PICHELIN, M., BALE, S. D., BELCHER, J. W., BERG, P., BERGNER, H., BERTHOMIER, M., BOOKBINDER, J. *et al.* 2015 Solar wind electrons alphas and protons (SWEAP) investigation: design of the solar wind and coronal plasma instrument suite for solar probe plus. *Space Sci. Rev.* **204**, 131–186.

KLEIN, K. G., HOWES, G. G., TENBARGE, J. M., BALE, S. D., CHEN, C. H. K. & SALEM, C. S. 2012 Using synthetic spacecraft data to interpret compressible fluctuations in solar wind turbulence. *Astrophys. J.* **755**, 159.

KOPP, R. A. & HOLZER, T. E. 1976 Dynamics of coronal hole regions. I – steady polytropic flows with multiple critical points. *Solar Phys.* **49**, 43–56.

LITHWICK, Y. & GOLDREICH, P. 2001 Compressible magnetohydrodynamic turbulence in interstellar plasmas. *Astrophys. J.* **562**, 279–296.

LITHWICK, Y., GOLDREICH, P. & SRIDHAR, S. 2007 Imbalanced strong MHD turbulence. *Astrophys. J.* **655**, 269–274.

MALARA, F., PRIMAVERA, L. & VELTRI, P. 2000 Nonlinear evolution of parametric instability of a large-amplitude nonmonochromatic Alfvén wave. *Phys. Plasmas* **7**, 2866–2877.

MALLET, A., SCHEKOCHIHIN, A. A. & CHANDRAN, B. D. G. 2015 Refined critical balance in strong Alfvénic turbulence. *Mon. Not. R. Astron. Soc.* **449**, L77–L81.

MANEVA, Y. G., VIÑAS, A. F. & OFMAN, L. 2013 Turbulent heating and acceleration of He^{++} ions by spectra of Alfvén-cyclotron waves in the expanding solar wind: 1.5-D hybrid simulations. *J. Geophys. Res. (Space Physics)* **118**, 2842–2853.

MARON, J. & GOLDREICH, P. 2001 Simulations of incompressible magnetohydrodynamic turbulence. *Astrophys. J.* **554**, 1175–1196.

MARSCH, E., ROSENBAUER, H., SCHWENN, R., MUEHLHAEUSER, K. & NEUBAUER, F. M. 1982 Solar wind helium ions – observations of the HELIOS solar probes between 0.3 and 1 AU. *J. Geophys. Res.* **87**, 35–51.

MARSCH, E. & TU, C.-Y. 1990 On the radial evolution of MHD turbulence in the inner heliosphere. *J. Geophys. Res.* **95**, 8211–8229.

MATTHAEUS, W. H. & GOLDSTEIN, M. L. 1986 Low-frequency $1/f$ noise in the interplanetary magnetic field. *Phys. Rev. Lett.* **57**, 495–498.

MEYRAND, R., KIYANI, K. H. & GALTIER, S. 2015 Weak magnetohydrodynamic turbulence and intermittency. *J. Fluid Mech.* **770**, R1.

NG, C. S. & BHATTACHARJEE, A. 1996 Interaction of shear-Alfven wave packets: implication for weak magnetohydrodynamic turbulence in astrophysical plasmas. *Astrophys. J.* **465**, 845.

PARKER, E. N. 1958 Dynamics of the interplanetary gas and magnetic fields. *Astrophys. J.* **128**, 664–676.

PEREZ, J. C. & CHANDRAN, B. D. G. 2013 Direct numerical simulations of reflection-driven, reduced MHD turbulence from the sun to the Alfven critical point. *Astrophys. J.* **776**, 124.

PODESTA, J. J. 2009 Dependence of solar-wind power spectra on the direction of the local mean magnetic field. *Astrophys. J.* **698**, 986–999.

RAYMOND, J. C., MCCAULEY, P. I., CRANMER, S. R. & DOWNS, C. 2014 The solar corona as probed by comet Lovejoy (C/2011 W3). *Astrophys. J.* **788**, 152.

SAGDEEV, R. Z. & GALEEV, A. A. 1969 *Nonlinear Plasma Theory*. W. A. Benjamin.

SCHEKOCHIHIN, A. A., NAZARENKO, S. V. & YOUSEF, T. A. 2012 Weak Alfvén-wave turbulence revisited. *Phys. Rev. E* **85** (3), 036406.

SCHEKOCHIHIN, A. A., PARKER, J. T., HIGHCOCK, E. G., DELLAR, P. J., DORLAND, W. & HAMMETT, G. W. 2016 Phase mixing versus nonlinear advection in drift-kinetic plasma turbulence. *J. Plasma Phys.* **82** (2), 905820212.

SHI, M., LI, H., XIAO, C. & WANG, X. 2017 The parametric decay instability of Alfvén waves in turbulent plasmas and the applications in the solar wind. *Astrophys. J.* **842**, 63.

SPANGLER, S. R. 1986 The evolution of nonlinear Alfven waves subject to growth and damping. *Phys. Fluids* **29**, 2535–2547.

SPANGLER, S. R. 1989 Kinetic effects of Alfven wave nonlinearity. I – ponderomotive density fluctuations. *Phys. Fluids* B **1**, 1738–1746.

SPANGLER, S. R. 1990 Kinetic effects on Alfven wave nonlinearity. II – the modified nonlinear wave equation. *Phys. Fluids* B **2**, 407–418.

SUZUKI, T. K. & INUTSUKA, S.-I. 2005 Making the corona and the fast solar wind: a self-consistent simulation for the low-frequency Alfvén waves from the photosphere to 0.3 AU. *Astrophys. J. Lett.* **632**, L49–L52.

TAYLOR, G. I. 1938 The spectrum of turbulence. *Proc. R. Soc. Lond.* A **164**, 476–490.

TENERANI, A., VELLI, M. & HELLINGER, P. 2017 The parametric instability of Alfvén waves: effects of temperature anisotropy. *Astrophys. J.* **851** (2), 99.

TERASAWA, T., HOSHINO, M., SAKAI, J.-I. & HADA, T. 1986 Decay instability of finite-amplitude circularly polarized Alfven waves – a numerical simulation of stimulated Brillouin scattering. *J. Geophys. Res.* **91**, 4171–4187.

Tu, C. & Marsch, E. 1995 MHD structures, waves and turbulence in the solar wind: observations and theories. *Space Sci. Rev.* **73**, 1–210.

Vasquez, B. J. 1995 Simulation study of the role of ion kinetics in low-frequency wave train evolution. *J. Geophys. Res.* **100**, 1779–1792.

Velli, M. 1993 On the propagation of ideal, linear Alfven waves in radially stratified stellar atmospheres and winds. *Astron. Astrophys.* **270**, 304–314.

Velli, M., Grappin, R. & Mangeney, A. 1989 Turbulent cascade of incompressible unidirectional Alfven waves in the interplanetary medium. *Phys. Rev. Lett.* **63**, 1807–1810.

Verdini, A., Grappin, R., Pinto, R. & Velli, M. 2012 On the origin of the $1/f$ spectrum in the solar wind magnetic field. *Astrophys. J. Lett.* **750**, L33.

Verdini, A., Velli, M., Matthaeus, W. H., Oughton, S. & Dmitruk, P. 2010 A turbulence-driven model for heating and acceleration of the fast wind in coronal holes. *Astrophys. J. Lett.* **708**, L116–L120.

Verscharen, D., Chandran, B. D. G., Bourouaine, S. & Hollweg, J. V. 2015 Deceleration of alpha particles in the solar wind by instabilities and the rotational force: implications for heating, Azimuthal flow, and the Parker spiral magnetic field. *Astrophys. J.* **806**, 157.

Yao, S., He, J.-S., Marsch, E., Tu, C.-Y., Pedersen, A., Rème, H. & Trotignon, J. G. 2011 Multi-scale anti-correlation between electron density and magnetic field strength in the solar wind. *Astrophys. J.* **728**, 146.

Zhou, Y. & Matthaeus, W. H. 1989 Non-WKB evolution of solar wind fluctuations: a turbulence modeling approach. *Geophys. Res. Lett.* **16**, 755–758.